Shock-Timing Experiments Using Double-Pulse Laser Irradiation

Introduction

Direct-drive inertial confinement fusion (ICF) targets use temporally shaped drive pulses to optimize the target performance while controlling the Rayleigh–Taylor instability.[1–3] The portion of the pulse preceding the main compression drive is used to create shocks that modify the target adiabat and thereby determine the compressibility and stability of the imploding shell. After the passage of the first shock, the compressed material at the ablation front relaxes to densities below solid, thereby increasing the ablation velocity produced by the main drive providing ablative stabilization.[4–6] Adiabat shaping[7] is a refinement that uses a short pulse (~100 ps) preceding the main pulse to produce an initial shock that is not supported and therefore decays as it propagates through the target shell. Ideally, this decaying shock produces a larger adiabat in the outer portion of the shell (where the shock is stronger) than the inner portion, simultaneously improving target stability and maintaining high compressibility of the main fuel.

An optimized direct-drive ICF implosion requires that the main compression wave overtake the first shock just as that shock reaches the inner surface of the cryogenic fuel layer.[8] (Ideally, the main drive should compress and implode the capsule isentropically. In ICF, this compression is so rapid and steep that it is sometimes referred to as a shock wave.) If the compression wave is too late, the first shock enters the fuel, prematurely compressing and heating it. If it is too early, the inner portion of the target is placed on too high an adiabat, reducing its compressibility. For direct-drive ignition target designs, the compression wave must overtake the first shock to within ±150 ps of the design specification.[9]

Indirect-drive ICF implosions are less susceptible to Rayleigh–Taylor instabilities and are therefore designed to implode along lower adiabats. Ignition designs for indirect drive use three shocks to moderately compress the target shell with a minimal increase to the adiabat before arrival of the compression wave (sometimes referred to as the fourth shock). Indirect-drive ignition target designs specify that the timing of the first three shocks be controlled to ±50 ps and the fourth shock be timed to ±100 ps.

In both of these cases, the target compression requires multiple shock waves to achieve optimal performance. The timing of those shocks is critical to that performance. It is therefore important that the simulation codes used to design ignition targets be validated with experiments that provide information on how multiple shocks propagate in laser-driven targets and provide the timing of those shocks. Experiments at the OMEGA[10] laser are conducted to develop the experimental techniques to do this and to validate direct-drive designs. Eventually, those techniques will be used on the National Ignition Facility (NIF)[11] to evaluate whether a given pulse shape meets the shock-timing specification.

We report on a series of experiments at the OMEGA Laser Facility that study the propagation and timing of multiple shocks in planar targets. In a direct-drive implosion, shock coalescence occurs before significant target motion, making the planar approximation valid. Planar targets are ideally suited to shock-wave experiments because they afford diagnostic access and because shocks can readily be produced at conditions that are relevant to ICF. These experiments demonstrate our ability to observe shock-velocity profiles and discern shock coalescence (timing) with the precision required for ignition targets. Hydrodynamic simulations of these experiments model the time history of the shock velocities and the observed coalescence times to the accuracies required for direct-drive ignition targets.

Experiments

The experiments were performed using planar 125-μm-thick polystyrene (ρ = 1.05 g/cc) targets that were directly irradiated with two 90-ps pulses separated by 1 to 2 ns with 12 OMEGA laser beams.[10] The shocks created by these pulses were observed using a velocity interferometer system for any reflector (VISAR)[12,13] that records the shock velocity as a function of time. The time-resolved optical emission from the shocks was simultaneously recorded. The experimental configuration shown in Fig. 104.17 where two rings of beams (six in each) are shown at their angles of incidence (23° and 48°). Each beam has a phase plate (DPP)[14] that produces a super-Gaussian intensity profile in space described by

$I(r) = I_0 \exp\left[-\left(r/412\ \mu m\right)^{4.7}\right]$, with I_0 being 1–5 × 10^{14} W/cm^2. Obliquity causes the 48° beams to produce a spot on the target that is elongated 40% more than the 23° beams. The rear side of the target is observed with an optical system that also conveys to the target a 532-nm probe beam for the VISAR. In the reverse direction, the reflected probe beam and the self-emission from the target are imaged onto streak cameras.

The experiments were performed with 90-ps pulses, approximately Gaussian in time, in two groups of six beams. Each group had the same angle of incidence (either 23° or 48°) and was timed so that one group arrived 1 to 2 ns later than the other. These produced two shock waves in the target that are initially separated by the beam delay. The strength and timing of the second drive pulse was arranged so the second shock overtook the first in the target, providing an observable shock-coalescence event. Experiments were performed with either the 23° beams or the 48° beams arriving first, and the relative energies of the two groups were varied. This article presents detailed results from six shots representative of many shock-timing experiments. The laser conditions for these shots are detailed in Table 104.I, which defines the energy and angle of incidence for the two groups of beams (six in each) for each shot number. The first group arrives at t = 0, and the arrival time of the second group is shown in the table. Each group comprises six beams oriented in hexagonal symmetry, so that for oblique angles of incidence, there is no directional bias. It should be noted that the laser spots (at normal incidence) were the same size for both sets of beams. As a result of obliquity, the 48° beams produce spots that are more elongated and therefore have, for similar energies, intensities that are 73% of the 23° beams. To accommodate this, the shots with the 48° beams first have the second group delayed an extra 0.5 ns to ensure that the coalescence signal could be observed after the blank out by the second pulse.

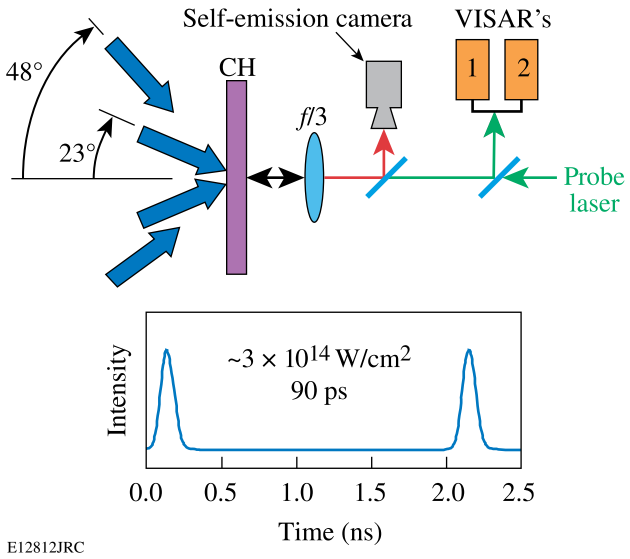

Figure 104.17
Experimental configuration with two short pulses, typically 1 to 2 ns apart. Beams arranged in two rings (having up to six beams each) at 23° and 48° irradiate solid polystyrene targets. A probe laser is image relayed by a *f*/3 telescope to the rear side of the target and reflected off a shock within the target into two VISAR diagnostics. The same telescope images the optical emission from the shock onto a streak camera.

These drive intensities produce ~10-Mb shocks that are hot (5,000–50,000 K), dense (2–4 times solid), and have steep gradients. At optical frequencies they are bright and reflective (30%–80%). VISAR has been demonstrated to be a very precise method for measuring shock velocities. It uses interferometry to measure the Doppler shift of a probe beam reflected off the shock front as it traverses the target.[12] A few percent precision in velocity with a time resolution of ~25 ps is routinely obtained.[13]

Table 104.I: Summary of beam-configuration information for shock-timing shots.

Shot #	1st group energy (J)	1st group angle (°)	2nd group delay (ns)	2nd group energy (J)	2nd group angle (°)
32208	120	23	1.5	258	48
32213	252	48	2.0	111	23
32214	111	48	2.0	240	23
32215	73	23	1.5	250	48
32216	119	23	1.5	258	48
32217	236	48	2.0	229	23

VISAR Experiments

VISAR is extensively used in laser-driven equation of state experiments[15–17] where aluminum "pushers" convey the shock into the sample. These pushers act as a standard reference and shield the samples from x rays from the coronal plasma that drives the shock. In contrast, ICF capsules usually contain only low-Z materials, so x rays from the corona readily propagate through the shell and fuel. The optical diagnostics used in shock-timing experiments performed with low-Z materials can be compromised by x rays that photoionize the target material ahead of the shock. This causes the material to become opaque to the VISAR probe laser, thus "blinding" the VISAR diagnostic during the laser pulse. After the drive ends, the ionized electrons recombine, the target transparency is restored, and the shock can again be observed. With short pulses, the diagnostic record is interrupted for only a few hundred picoseconds during each laser pulse and a nearly complete shock-velocity record is obtained.

Figure 104.18 shows the VISAR record for shot 32213 having 240 J in the first group of beams incident at 48° and 111 J in the second (at 23°) that arrived 2 ns later. This figure is a streak-camera record of the VISAR fringes as a function of time with the vertical dimension corresponding to the spatial direction transverse to the drive laser (and shock) propagation direction. The fringes are deliberately superposed on the image of the target and serve as a phase reference, i.e., zero velocity. (In this case, the early signal results from reflection off the front surface of the transparent target; the rear surface has an antireflection coating). For $t < 0$, the fringes are horizontal (constant phase) because the target is not moving. At $t = 0$, the first pulse irradiates the target, forming a coronal plasma on the front side of the target and producing a shock that propagates into the target. The data record shows, that during the laser pulse, x-ray photoionization causes absorption attenuation of the VISAR laser light to below the detection threshold. After the pulse, by $t \sim 0.5$ ns, the target transmissivity rises and the VISAR signal (fringes) are again detected. During this time, a rapidly changing fringe pattern is observed. The fringe position is proportional to the velocity of the reflecting surface (the shock), so the curvature of the fringes represents the decay of the shock velocity as it propagates through the target.

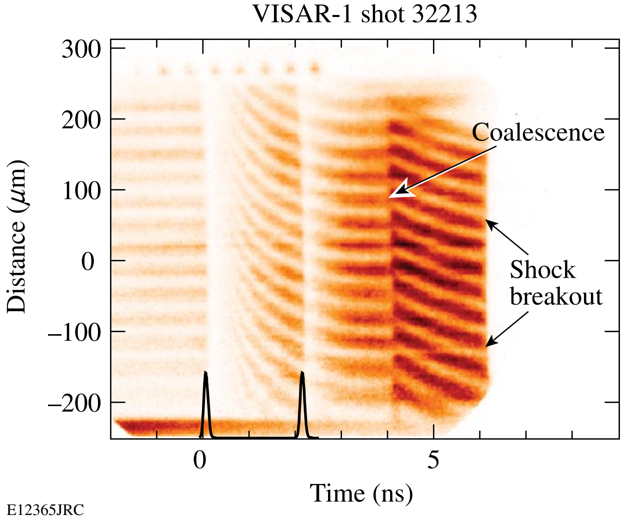

Figure 104.18
Temporally resolved VISAR record from shot 32213 (see text). The fringes are initially horizontal (zero velocity) until they disappear at $t = 0$ because of x-ray ionization in the target bulk. Upon reappearance, they have a curvature that results from the decreasing velocity of an unsupported first shock wave that decays as it propagates through the target. At 2 ns, the second laser pulse produces another burst of ionization, blanking the signal again. At ~4 ns, the second shock overtakes the first and the VISAR fringes have a discontinuous jump in position, brightness, and curvature. This coalesced shock also decays and finally reaches the rear surface (breakout) at ~6.2 ns, at which time the VISAR signal ceases.

At 2 ns, the second pulse irradiates the target. X rays produced by that pulse blind the diagnostic again and the fringes disappear. When the target recovers from the second pulse (at ~3 ns) the fringe record is still due to reflection off the first shock because the first shock is still ahead of the second shock and nearer to the VISAR. (Note the continuity in the slope of the fringes before and after arrival of the second pulse at 2 ns.) The first shock ionizes the CH above the critical density of the probe beam, ensuring that the probe is reflected and preventing the second shock from being "seen" through the first.

The record from ~0.5 ns to 4.0 ns shows the expected monotonic decay[18] of an unsupported shock traversing the target. At 4 ns, the second shock catches up to the first shock, forming a single coalesced shock that is stronger, and therefore faster, than the first shock. This event is recorded as a discontinuous jump in the fringe position (an increase in velocity) and an increase in the VISAR signal that is due to a concomitant jump in reflectivity for the stronger shock. The coalesced shock is also unsupported; it decays as shown by the curvature in the fringe pattern after 4 ns. The fringes from the coalesced shock persist until that shock reaches the rear surface of the target. At this point the shock "breaks out" and the rear surface releases into vacuum. These shocks produce temperatures and pressures sufficient to melt the CH, so as it releases, the material vaporizes, forming a density profile that quickly absorbs the probe laser and the VISAR signal disappears.

In this experiment, the second shock overtook the first shock despite being driven by half the energy of the first. This is the result of the increased sound speed and the particle velocity in the shock material. In the laboratory frame, one must add the particle velocity to the second shock velocity. Shock waves are supersonic relative to the unshocked material but subsonic relative to the shocked material. This is why rarefaction waves, which travel at the sound speed in the shocked material, can overtake shock waves.

Another interesting feature is the temporal rise of the signal intensity, as seen, for example, in Fig. 104.18 from 0.5 ns to 2 ns. The intensity of the VISAR fringes depends on the amount of reflection from the shock; typically, stronger shocks produce more free electrons and therefore have higher reflectivity. The gradual rise noted in Fig. 104.18 results not from increased reflectivity at the shock front because its reflectivity diminishes with decreasing velocity. Instead, the increase results from a decreased path length of the probe beam through the attenuating material as the shock moves toward the rear of the target.

Figure 104.19 shows the velocity profiles derived from the VISAR data recorded during two similar experiments. The solid line is the velocity profile from a two-pulse experiment (#32216) having 119 J in the first pulse (from beams at 23°) and, 1.5 ns later, 258 J (from beams at 48°). The initial shock is observed starting at ~0.3 ns and can be seen to decay continuously until 3.5 ns, when the velocity jumps because the second shock has overtaken it. That coalesced shock then decays and eventually reaches the end of the target at 5 ns. The dashed curve in Fig. 104.19 is the velocity profile for an identical experiment (shot 32215) except that the first pulse has only 75 J. The initial shock (0.3 to ~3 ns) has a lower velocity and, as a result, the second shock overtakes it earlier (at 2.9 ns). Note also that the coalesced shock is stronger (higher velocity) than the coalesced shock in shot 32216 because the second shock overtakes the first shock sooner (earlier in the decay of the shock).

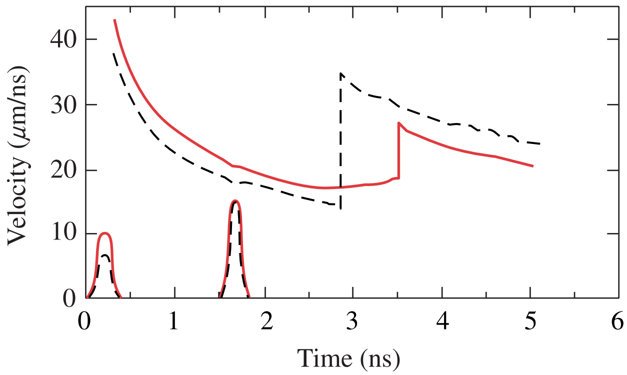

Shots:32215 & 32216
E12534JRC

Figure 104.19
The shock-velocity history derived from the VISAR data for shots 32216 (solid) and 32215 (dashed). In both cases the target was irradiated by six beams at 23° and 1.5 ns later, by six beams at 48°. For shot 32166, the first group contained 119 J and the second 258 J. Shot 32215 had 73 J and 250 J, respectively. For shot 32216, the VISAR records the velocity of only the first shock until ~3.5 ns when the second shock overtakes the first. After the shocks coalesce, the velocity recorded by VISAR jumps. In the dashed curve, the catch-up occurs earlier because the initial shock is slower (lower first-pulse energy) and the jump is higher because the second shock has had less time to decay.

When the driving pressure behind a shock relaxes, the shock wave will begin to decay. This occurs because the material behind the shock (that is both heated and compressed) begins to rarefy. In a laser-driven shock that rarefaction begins at the coronal and propagates toward the shock at the local sound speed that is higher than the shock speed. When the rarefaction wave reaches the shock it causes the shock strength to decay at a rate that is proportional to the rarefaction rate. Note that in both experiments shown in Fig. 104.19, the first shock decays more rapidly than the coalesced shock. This is because the first shock traversed less material and hence the rarefaction rate is faster than for the second and coalesced shocks that encountered more material.

In another experiment, the timing of the pulses was reversed (i.e., 48° beams first). Figure 104.20 shows a comparison of the velocity profiles for the two cases. The solid curve is shot 32216 that has the 23° beams first (see solid curve in Fig. 104.19 and its description), and the dashed curve is shot 32214 with 111 J in the 48° beams first and 240 J in the 23° beams second. For the latter, the interbeam timing was lengthened to 2 ns so that the coalescence occurs after the blank out caused by the second pulse. It can be seen that the 48° beams produce a first shock that has 70% of the velocity of that produced by the 23° beams. This is because the 48° beams produce lower intensity and couple less efficiently to the target. In the dashed curve, the slower first-shock velocity reduces the coalescence time despite having the second pulse delayed by 0.5 ns with respect to the other case. The second shock (here produced by the 23° beams) creates a larger jump in velocity for the coalesced shock. This occurs because the 23° beams have a higher intensity and couple more efficiently, thus producing a stronger (and faster) shock.

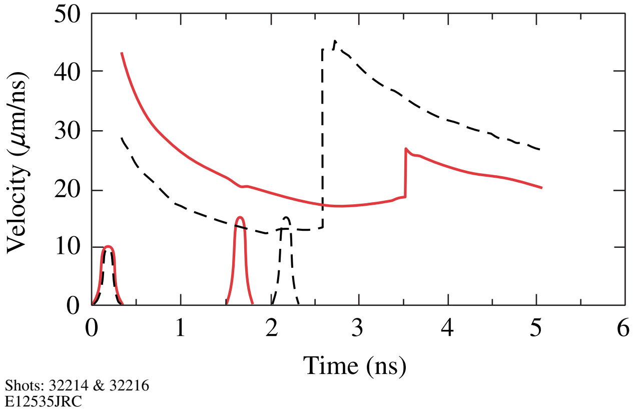

Figure 104.20
Velocity profiles from shot 32216 with 23° then 48° beams (solid) and 32214 (dashed) where the beam timing is reversed (48° beams first). Note that for similar drive energies, the first shock velocity is lower in the latter case. This is because the 48° beams couple less efficiently than the 23° beams. The velocity jump at coalescence is higher because the 23° beams produce a stronger shock.

To obtain the velocity records, the fringe position (phase) as a function of time must be determined. The sensitivity of fringe displacement to velocity is set by the length of the delay etalon in the VISAR interferometer and by the refractive index of the target material (polystyrene $n = 1.59$). VISAR can produce velocity measurements with accuracies of ~1% based on the ability to detect shifts of about 1/20 of a fringe and because the actual shifts are 3 to 5 fringes. We found that ionization has negligible effect on VISAR sensitivity. We estimated the ionized (or free) electron density using the loss of the VISAR signal as a measure of the absorption coefficient model to infer changes to the refractive index. Ionization fractions of ~0.02 would cause 100 times attenuation of the signal yet result in only a few percent change in the refractive index. Recent experiments have confirmed that severe ionization blanking occurred in polystyrene with only negligible changes in the index of refraction.[20] Preliminary studies of x-ray–induced ionization blanking indicate that, in addition to absorption by free electrons, valance-band vacancies play a role in the absorption of the probe beam. In Figs. 104.19 and 104.20, the experimental velocity profiles for the first shock show negligible change in the slope across the interruption caused by second pulse. Thus, despite large changes in signal level, the inferred velocity profile is negligibly changed.

Self-Emission Measurements

Simultaneous with the VISAR measurements, temporal records of the self-emission (600–1000 nm) from the shocks were acquired using an imaging streak camera with an S20 photocathode.[21] Figure 104.21(a) shows the VISAR record for shot 32208 with the corresponding record of the spatially and temporally resolved self-emission intensity shown in Fig. 104.21(b). This shot has 120 J in first pulse at 23° and 260 J 1.5 ns later at 48°. The spatial resolution of VISAR and the self-emission monitor are along the same direction (vertical on target). The distinct shock coalescence and breakout features discussed above are readily evident in both images. In Fig. 104.21(b), the onset of emission from the shock occurs at ~0.7 ns as an intense planar feature whose intensity decays nearly to the background level at ~3 ns. At about 3.2 ns, the emission suddenly reappears when the second shock overtakes the first and the coalesced shock produces a stronger emission. The abrupt temporal

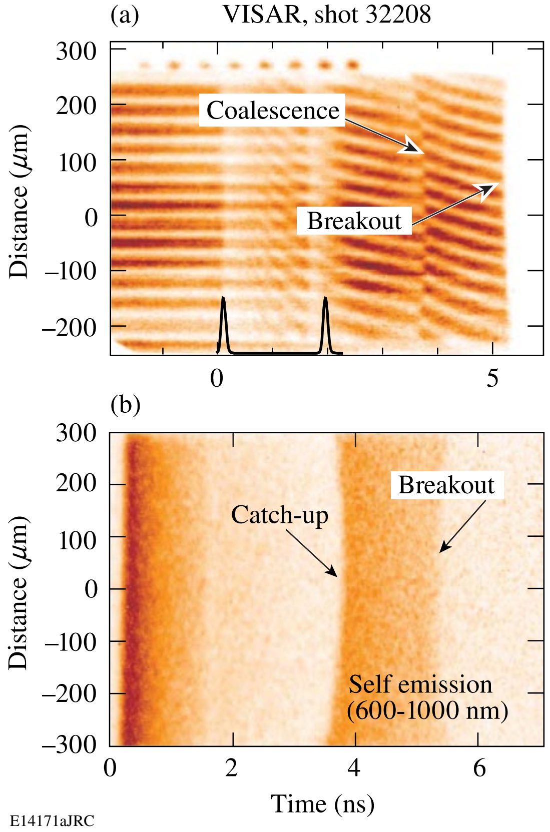

Figure 104.21
(a) The VISAR record and (b) the time-resolved optical self-emission profile for shot 32208. The velocity, catch-up, and breakout features that are seen in the VISAR record are also seen in the self-emission. At about 0.3 ns, the emission from the first shock is visible first, then it decays as the shock velocity decays. At catch-up (~4 ns) the coalesced shocks produce an emission that is again bright. This decays until breakout where emission ceases. The curvature of the catch-up and breakout features is related to the spatial shapes of the shock fronts.

onset of the emission from the coalesced shock indicates that the second (brighter) shock cannot be "seen" through the first shock. Again, this is because the first shock produces material that is overdense for these wavelengths.

For shock velocities of 15 to 40 μm/ns in polystyrene, the shock temperature ranges from 1 to 8 eV and depends quadradically on shock velocity. This dependence causes the self-emission intensity to drop rapidly. It falls below the detection threshold of the device for a portion of the record. These self-emission profiles corroborate the features seen in the velocity profiles. The shock catch-up and breakout times measured by each of the diagnostics agree, and the velocity profiles can be confirmed using the intensity profile as a reference.

In Figs. 104.21(a) and 104.21(b) (and Fig. 104.18 as well), the catch-up and breakout are curved; this curvature provides insight into the two-dimensional behavior of these experiments. The shock-breakout feature in these experiments is curved; the center breaks out before the edges. The curvature is a result of edge effects and velocity dispersion as the shock propagates to the rear of the target. At its edges, the shock has lower pressure because the laser is less intense, and lateral rarefaction waves move into the shock front. As a result, the shock front becomes curved as it propagates. The slower edges take longer to reach the rear surface of the target with respect to the more intense center. The result is the curved breakout signal.

In contrast, note that the coalescence signal in Fig. 104.21 has a curvature opposite of that at breakout. This is a result of the relative planarity of the two shocks. For shot 32208, the first shock was produced by the 23° beams that have a slightly smaller spot and therefore produce a shock with more curvature than that created by the larger spot because of the 48° beams. At coalescence, the flatter second shock overtakes the curved first shock, first at the edges and last at the center. The result is a catch-up signature that is curved opposite of the breakout, as in Figs. 104.21(a) and 104.21(b). In the cases where the 48° beams were first, the catch-up signal was observed to be flat or curved the other way.

Figure 104.22(a) shows the correlation of coalescence and breakout features as measured from the VISAR and self-emission records for shot 32217. The solid lines are the space-time locations of the coalescence and breakout features measured with VISAR, and the dotted lines are those determined from the self-emission record. Figure 104.22(b) is a comparison of the coalescence and breakout times derived from VISAR and self-emission for several shots over a range of detection times.

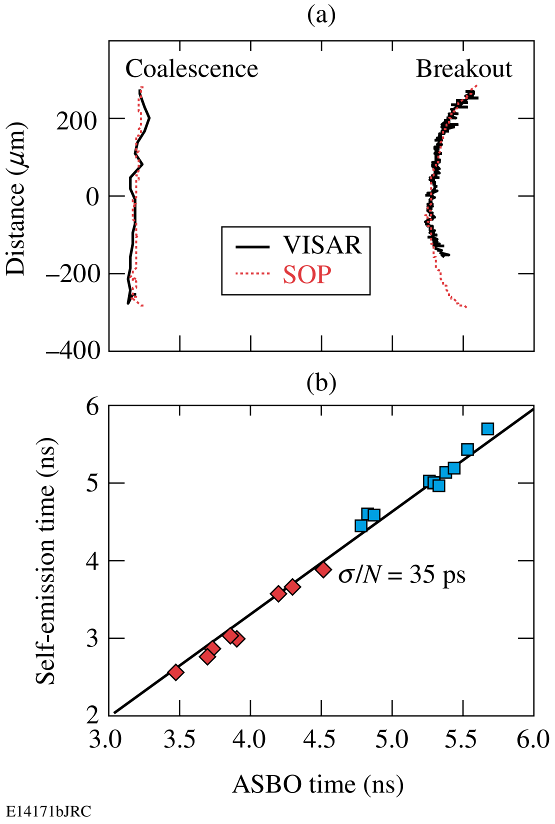

Figure 104.22
(a) Correlation of coalescence and breakout features in VISAR and self-emission data. (b) Correlation of the coalescence and breakout times as measured by VISAR and self-emission. These times agree to about the precision of the shock measurement.

Note that the correlation (±35 ps) is of the order of the accuracy of the VISAR measurements (±25 ps).

Simulations

Simulations of these experiments were performed using the one-dimensional hydrodynamics code *LILAC*.[22] Experimental conditions for the laser and target were inputs and the *SESAME*[23] equation of state was used for the polystyrene. The shock trajectories were found by tracking the shock position defined as the steepest gradient in the pressure. Figure 104.23 shows the velocity profiles from the simulations compared to the velocity profiles measured with VISAR. Figure 104.23(a) shows shot 32215 and Fig. 104.23(b) shows shot 32216. Note that the overall profiles are well modeled, as are the catch-up and breakout times. The simulations used a flux limiter of *f* = 0.06.[24] The effect of the different incident angles uses an algorithm that analytically treats ray tracing in density gradients to provide path length and absorption information to the one-dimensional code.[25] For six such shots, the simulations were able to predict the shock coalescence and breakout times to better than ±150 ps, the required precision needed for the timing of the shock in direct-drive ignition targets.

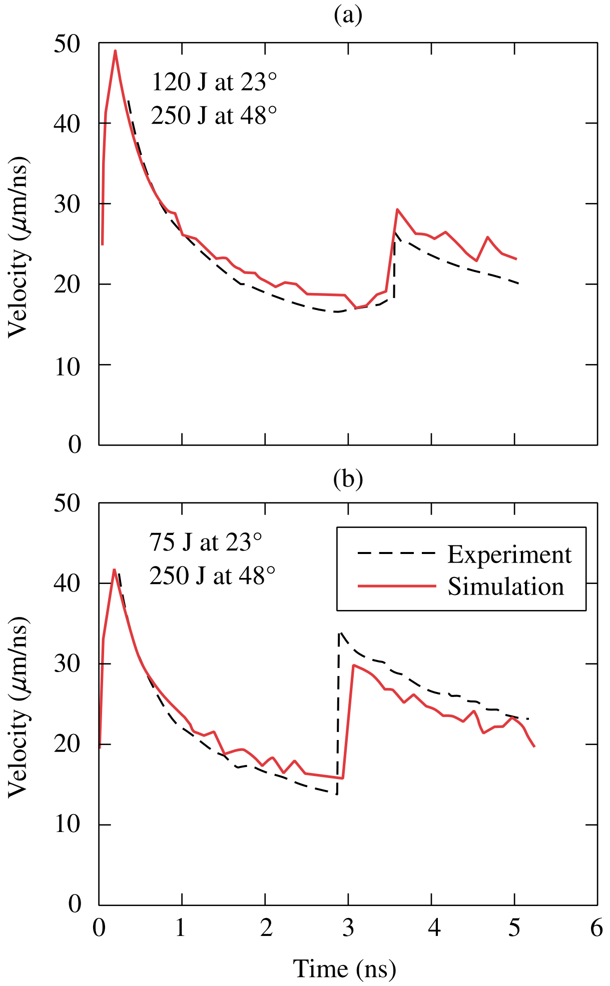

E12536JRC

Figure 104.23
Comparison of measured (solid) and simulated (dashed) velocity profiles for (a) shot 32215 and (b) shot 32216. The measured velocities are well modeled, including the catch-up times where the shocks coalesce and the breakout times where the shocks reach the rear surface of the target.

Angle of Incidence

In a similar series of experiments, the effect of the incident angle was studied by inferring the peak shock pressure produced by beams at various angles. The velocity profiles of decaying shocks produced by beams at 23°, 48°, and 62° were compared. The velocity profiles of the decaying shocks were fit to models for unsupported shock waves,[7,18] and the results were used to infer the peak pressure produced by these pulses. The single-drive pulses were 90 ps in duration and the energy or numbers of beams were changed to vary the incident intensity.

Figure 104.24 shows a plot of the inferred peak pressure versus the incident laser intensity. The experimental results for the three angles are shown as solid figures and the simulations of those experiments as open figures. The experiments for 23° produce a larger range of pressures because they have smaller spots and couple more efficiently. The solid line is a power-law fit to the pressure where $P \propto I^{0.65}$, in agreement with established intensity scaling of $P \propto I^{2/3}$ (Ref. 26). Note that the simulations predict the effect of the incident angle quite well.

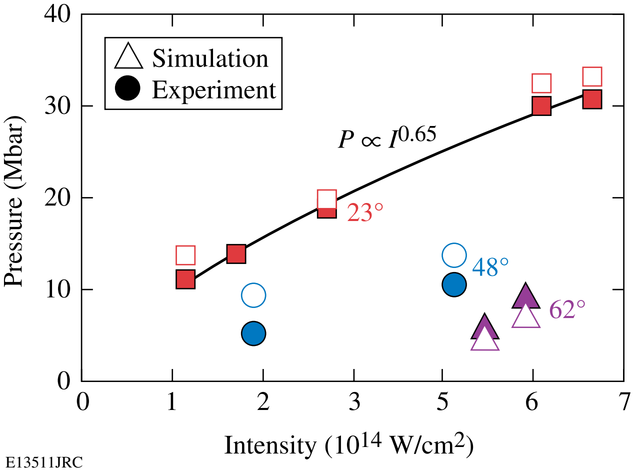

E13511JRC

Figure 104.24
Peak shock pressure versus incident laser intensity for beams at incident angles of 23°, 48°, and 62°. The experimental peak pressure (solid points) was inferred from the measured velocity profile using a model for the decay of an unsupported shock wave. The simulated peak pressures are shown as open points. The solid line is a simple power-law scaling for the intensity dependence of pressure.

Conclusions

The velocity profiles of multiple shocks in planar targets irradiated by two short pulses have been measured using VISAR and self-emission data. The deduced velocity profiles show the shocks propagating through the targets and exhibit clear evidence of the time that the second shock overtakes the first. The coalescence times and the arrival of the coalesced shocks at the rear side of the targets are clearly observed and corroborated by the self-emission data. Shock timing and breakout were measured with accuracies of better than ±50 ps. The spatial shape of the catch-up and breakout signals exhibit features that are attributed to two-dimensional effects caused largely by the finite size of the drive pulses.

The velocity profiles and shock timing are well modeled by one-dimensional hydrodynamics codes that include ray tracing to account for oblique incidence. The simulations predict shock timing and breakout to better than ±150 ps, the required precision for direct-drive ignition targets. These results demonstrate our ability to measure and model the behavior of multiple laser-driven shocks propagating in planar targets irradiated by double laser pulses and provide confidence in the hydrodynamic codes used for to design inertial confinement fusion targets.

These double-pulse experiments will be extended to cryogenic deuterium targets and continuous laser pulses. Similarly, experiments will also be performed with indirect-drive ICF to study the behavior and timing of three shocks driven by hohlraums. These experiments on OMEGA will be used to develop techniques that ultimately will be used to fine-tune targets and pulse shapes for ignition experiments on the NIF.

ACKNOWLEDGMENTS

This work was supported by the U.S. Department of Energy Office of Inertial Confinement Fusion under Cooperative Agreement No. DE-FC03-92SF19460, the University of Rochester, and the New York State Energy Research and Development Authority. The support of DOE does not constitute an endorsement by DOE of the views expressed in this article.

REFERENCES

1. J. D. Lindl, Phys. Plasmas **2**, 3933 (1995).
2. S. E. Bodner, D. G. Colombant, J. H. Gardner, R. H. Lehmberg, S. P. Obenschain, L. Phillips, A. J. Schmitt, J. D. Sethian, R. L. McCrory, W. Seka, C. P. Verdon, J. P. Knauer, B. B. Afeyan, and H. T. Powell, Phys. Plasmas **5**, 1901 (1998).
3. J. D. Kilkenny, S. G. Glendinning, S. W. Haan, B. A. Hammel, J. D. Lindl, D. Munro, B. A. Remington, S. V. Weber, J. P. Knauer, and C. P. Verdon, Phys. Plasmas **1**, 1379 (1994).
4. H. Takabe, L. Montierth, and R. L. Morse, Phys. Fluids **26**, 2299 (1983).
5. R. Betti, V. N. Goncharov, R. L. McCrory, P. Sorotokin, and C. P. Verdon, Phys. Plasmas **3**, 2122 (1996).
6. S. E. Bodner, Phys. Rev. Lett. **33**, 761 (1974).
7. K. Anderson and R. Betti, Phys. Plasmas **10**, 4448 (2003).
8. P. W. McKenty, V. N. Goncharov, R. P. J. Town, S. Skupsky, R. Betti, and R. L. McCrory, Phys. Plasmas **8**, 2315 (2001).
9. *Proposal for Renewal Award for Cooperative Agreement DE-FC03-92SF-19460*, Between the U.S. Department of Energy and the Laboratory for Laser Energetics of the University of Rochester, Addendum: Response to Reviewers' Questions (Rochester, NY, 2001).
10. T. R. Boehly, D. L. Brown, R. S. Craxton, R. L. Keck, J. P. Knauer, J. H. Kelly, T. J. Kessler, S. A. Kumpan, S. J. Loucks, S. A. Letzring, F. J. Marshall, R. L. McCrory, S. F. B. Morse, W. Seka, J. M. Soures, and C. P. Verdon, Opt. Commun. **133**, 495 (1997).
11. J. D. Lindl *et al.*, Phys. Plasmas **11**, 339 (2004).
12. L. M. Barker and R. E. Hollenbach, J. Appl. Phys. **43**, 4669 (1972).
13. P. M. Celliers, D. K. Bradley, G. W. Collins, D. G. Hicks, T. R. Boehly, and W. J. Armstrong, Rev. Sci. Instrum. **75**, 4916 (2004).
14. Y. Lin, T. J. Kessler, and G. N. Lawrence, Opt. Lett. **20**, 764 (1995).
15. G. W. Collins *et al.*, Science **281**, 1178 (1998).
16. M. Koenig, E. Henry, G. Huser, A. Benuzzi-Mounaix, B. Faral, E. Martinolli, S. Lepape, T. Vinci, D. Batani, M. Tomasini, B. Telaro, P. Loubeyre, T. Hall, P. Celliers, G. Collins, L. DaSilva, R. Cauble, D. Hicks, D. Bradley, A. MacKinnon, P. Patel, J. Eggert, J. Pasley, O. Willi, D. Neely, M. Notley, C. Danson, M. Borghesi, L. Romagnani, T. Boehly, and K. Lee, Nucl. Fusion **44**, S208 (2004).
17. T. R. Boehly, D. G. Hicks, P. M. Celliers, T. J. B. Collins, R. Earley, J. H. Eggert, D. Jacobs-Perkins, S. J. Moon, E. Vianello, D. D. Meyerhofer, and G. W. Collins, Phys. Plasmas **11**, L49 (2004).
18. R. J. Trainor and Y. T. Lee, Phys. Fluids **25**, 1898 (1982).
19. P. Drude, Ann. Phys. **1**, 566 (1900); N. W. Ashcroft and N. D. Mermin, *Solid State Physics*, College ed. (W.B. Saunders, Philadelphia, 1976).
20. W. Theobald, J. E. Miller, T. R. Boehly, E. Vianello, I. V. Igumenshchev, V. N. Goncharov, A. V. Maximov, and T. C. Sangster, Bull. Am. Phys. Soc. **50**, 347 (2005).
21. J. A. Oertel *et al.*, Rev. Sci. Instrum. **70**, 803 (1999).
22. J. Delettrez, R. Epstein, M. C. Richardson, P. A. Jaanimagi, and B. L. Henke, Phys. Rev. A **36**, 3926 (1987).
23. G. I. Kerley, J. Chem. Phys. **73**, 469 (1980).
24. R. C. Malone, R. L. McCrory, and R. L. Morse, Phys. Rev. Lett. **34**, 721 (1975).
25. M. Born and E. Wolf, *Principles of Optics: Electromagnetic Theory of Propagation, Interference and Diffraction of Light*, 5th ed. (Pergamon Press, Oxford, 1975).
26. J. D. Lindl, *Inertial Confinement Fusion: The Quest for Ignition and Energy Gain Using Indirect Drive* (Springer-Verlag, New York, 1998), Chap. 5, p. 54.